Paper 10S-03
WSS/CI Spring 2010 Meeting, Boulder, CO

Characterization of laminar flame propagation for non-unity Lewis number mixtures

M. S. Day, A. J. Aspden and J. B. Bell

Lawrence Berkeley National Laboratory, Berkeley, CA 94720, USA

Abstract

Turbulent premixed lean hydrogen-air mixtures at different equivalent ratios present significantly different behavior despite having the same Karlovitz and Damköhler numbers. The reason for this discrepancy is related to the thermodiffusively unstable nature of the flames, which drives the robust formation of cellular burning patterns. As a result, the natural propagation mode of these flames is not well characterized by the one-dimensional flat unstrained flame idealization used to derive the flame properties that normalize the Karlovitz and Damköhler numbers. This paper considers refining the definitions of the dimensionless parameters of turbulence-flame interaction using parameters that more appropriately characterize the freely-propagating structure of these flames. We perform three-dimensional simulations of freely-propagating flames over a range of equivalence ratios, and use data from those simulations to define modified Karlovitz and Damkölher numbers. We then perform a series of turbulent flame simulations that demonstrate that these redefinitions effectively eliminate the observed dependence on equivalence ratio.

1 Background

There has been considerable recent interest in the combustion of lean hydrogen-air and hydrogen-enriched lean hydrocarbon fuels. Such mixtures can be obtained, for example, from the gasification of coal or biomass and are potentially attractive alternatives to direct petroleum combustion, primarily due to their reduced flame temperature. Cooler exhaust streams result in extremely low rates of thermal NO_x production, offering potential solutions to extremely demanding and tightening emissions standards. However, there are a number of technological challenges to burning such fuels. In addition to a wide range of practical engineering and safety concerns, hydrogen-rich mixtures have the property that they tend to burn in localized cellular structures rather than in a continuous flame sheet typical of more traditional fuels such as natural gas and propane. Such "broken" surfaces, even in the low turbulence, laminar or freely-propagating scenarios, confound the broad range of theoretical models for flame transport, as practical modeling frameworks that have been developed for combustion engineering design and analysis.

Cellular burning modes are attributed directly to the disparity in heat and mass diffusivities of the fuel species, and have been studied over the years since the early works of Markstein [1] and Zeldovich [2]. More recently, hydrogen-based fuels have become the research topic of many researchers (see, for example, [3] and [4]). Interestingly, the cellular burning features in these systems are extremely robust. Significant levels of turbulent fluctuations in the fuel stream appear to have little effect on whether these features appear, as shown in experimental OH-PLIF images in [5], for example. This observation can be potentially devastating to the ultimate practical utility of hydrogen-rich fuels, since the burning cells appear to coincide with local "hot-spots", or regions of "super-adiabatic" thermal conditions. These hot-spots then support a locally elevated production of NO_x emissions which may be responsible for the NO_x "floor" observed in recent hydrogen-air flame experiments [6].

Given that the cellular burning patterns in thermodiffusively unstable flames result from molecular diffusion effects, it is reasonable to ask whether such behavior will disappear in the presence of extremely high levels of turbulence. An alternative is that high levels of turbulence will enhance transport in such a way that the flames simply extinguish. In fact, little is known about the behavior of lean H_2 flames across a broad range of turbulence intensities, and in particular, the extent to which the high diffusivity of H_2 competes with turbulent transport across the wide range of length, time and velocity scales.

The dimensionless Karlovitz and Damköhler numbers

$$\mathrm{Ka}_L^2 = \frac{\check{u}^3}{s_L^3}\frac{l_L}{l} \quad \text{and} \quad \mathrm{Da}_L = \frac{s_L}{\check{u}}\frac{l}{l_L}$$

are used to normalize the characterizing parameters of isotropic turbulence relative to properties relevant to a specific flame propagating within it. Here $\check{u}$ and l are the turbulent rms velocity and integral length scale, respectively, of fluctuations in the unburned fuel, and s_L and l_L are the propagation speed and thermal width of the flame, as measured in an idealized one-dimensional steady configuration that is free of mean strain or curvature (the so-called "flat laminar flame"). s_L and l_L vary considerably with equivalence ratio, even for a specific fuel type.

Aspden *et al.* [7] considered detailed numerical simulations of lean H_2-air flames across a range of turbulence conditions and fuel mixtures. The study included a set of flames at a fixed $\mathrm{Ka}_L = 1560$ and $\mathrm{Da}_L = .0047$; a snapshot of four such flames, with $\varphi = 0.31, 0.34, 0.37$ and 0.40, appear in figure 1. These cases are labelled D31, D34, D7 and D41, respectively, and have associated Lewis numbers that range 0.35 to 0.365. The values of Ka_L and Da_L were selected for these cases in order to guarantee that the flames were clearly in the "distributed reactions zone". The images represent slice planes taken parallel to the downward propagation direction of statistically steady flame brushes. These flames are embedded in a flow that is stirred by long-wavelength, zero-mean, isotropic forcing modes that drive the inertial-range cascade of isotropic turbulent fluctuations. The magnitude of the forcing determines the intensity of the turbulence, $\check{u}$, whereas the domain size, L determines the integral scale, $l = L/10$. The domains are periodic in the directions normal to the mean flame propagation. The upper boundary is "outflow", the lower boundary is isothermal free-slip, and both the upper and lower simulation boundaries are far from the flame (the computational domain there has an 8:1:1 aspect ratio to allow the flames to establish a steady propagation speed and then subsequent evolution to gather statistics of the burning). The model used to evolve these flames, including the conservation equations, chemical kinetics, transport properties and thermodynamics are identical to one that we will discuss below for additional studies presented in this paper.

In spite of occupying the same spot on the regime diagram, the flames shown in figure 1 are clearly exhibiting very different burning behavior. At the low equivalence ratio, there is a sharp interface between fuel and products, the turbulence is unable to disrupt the internal structure of the flame, and the burning occurs in small-scale structures across a broad flame brush. Regardless of the formal regime classification, this case is burning phenomenologically in the thin reaction zone regime. As the equivalence ratio increases (keeping both Ka_L and Da_L fixed), the turbulence has an increasing impact on the observed flame structure. At $\varphi = 0.4$, there no longer is a sharp interface between the fuel and products, and the burning occurs at the high temperature end of the flame. This flame is burning in the distributed burning regime (see [7] for more details).

For constant Ka_L we would expect the burning behavior of the flames to be roughly similar, but it appears that for low Lewis number flames, the turbulence-chemistry interaction regime is affected significantly by the equivalence ratio. This observation suggests that the Karlovitz number and Damköhler number based on laminar values do not accurately capture the effect of turbulence on low Lewis number flames. This paper proposes to rectify this shortcoming by replacing the laminar flame properties with freely-propagating values that provide a more accurate reflection of the flame speed and width that competes with the turbulence.

These freely-propagating values can then be used to construct modified Karlovitz and Damköhler numbers

$$\mathrm{Ka}_F^2 = \frac{\check{u}^3}{s_F^3}\frac{l_F}{l} \quad \text{and} \quad \mathrm{Da}_F = \frac{s_F}{\check{u}}\frac{l}{l_F},$$

where the suffix F is used to denote freely-propagating values. Here, we describe an approach to evaluating s_F and l_F and then perform a new set of simulations for a fixed Ka_F and Da_F to test our hypothesis.

2 Computational Methodology

The simulations presented here are based on a low Mach number formulation of the reacting flow equations. The methodology treats the fluid as a mixture of perfect gases. We use a mixture-averaged model for differential species diffusion and ignore Soret, Dufour, gravity and radiative transport processes. With these assumptions, the low Mach number equations for an open domain are

$$\begin{aligned}
\frac{\partial(\rho\boldsymbol{u})}{\partial t} + \nabla\cdot(\rho\boldsymbol{u}\boldsymbol{u}) &= -\nabla\pi + \nabla\cdot\tau, \\
\frac{\partial(\rho Y_i)}{\partial t} + \nabla\cdot(\rho Y_i\boldsymbol{u}) &= \nabla\cdot(\rho\mathcal{D}_i\nabla Y_i) + \dot{\omega}_i, \\
\frac{\partial\rho}{\partial t} + \nabla\cdot(\rho\boldsymbol{u}) &= 0, \\
\frac{\partial(\rho h)}{\partial t} + \nabla\cdot(\rho h\boldsymbol{u}) &= \nabla\cdot\left(\frac{\lambda}{c_p}\nabla h\right) + \\
&\quad \sum_i \nabla\cdot\left[h_i\left(\rho\mathcal{D}_i - \frac{\lambda}{c_p}\right)\nabla Y_i\right],
\end{aligned}$$

where ρ is the density, $\boldsymbol{u}$ is the velocity, Y_i is the mass fraction of species i, h is the enthalpy of the gas mixture, and $\dot{\omega}_i$ is the net production rate for species i due to chemical reactions. Also, λ is the thermal conductivity, τ is the stress tensor, c_p is the specific heat of the mixture, and $h_i(T)$ and $\mathcal{D}_i$ are the enthalpy and species mixture-averaged diffusion coefficients of species i, respectively where T denotes temperature. These evolution equations are supplemented by an equation of state for a perfect gas mixture.

The basic discretization combines a symmetric operator-split treatment of chemistry and transport with a density-weighted approximate projection method. The projection method incorporates the equation of state by imposing a constraint on the velocity divergence. The resulting system is integrated with time steps determined by the relatively slow advective transport. Advection is treated explicitly. Faster diffusion and chemistry processes are treated time-implicitly. This integration scheme is embedded in a parallel adaptive mesh refinement algorithm framework based on a hierarchical system of rectangular grid patches. The complete integration algorithm is second-order accurate in space and time, and discretely conserves species mass and enthalpy. The transport coefficients, thermodynamic relationships and hydrogen kinetics (chemical source terms) are obtained from the GRIMech 2.11 model [8] with the relevant carbon species removed. The reader is referred to [9] for details of the low Mach number model and its numerical implementation, and to [10] for previous applications of this methodology to the simulation of premixed turbulent flames.

3 Freely-Propagating Flames

To establish freely-propagating flame speeds and thermal widths, a simulation was run for each equivalence ratio $\varphi = 0.31$, 0.34, 0.37 and 0.4. In each case, a downward-propagating flame was simulated in a domain with a 3cm square cross-section, and a height of 9cm. Uniform inflow was specified at the lower

boundary, and the active control algorithm described in [11] was used to keep the flame at a statistically-steady height above the inlet. Lateral periodic boundaries were used, with outflow at the top of the domain. A base grid of $128 \times 128 \times 384$ was supplemented by two levels of refinement with refinement ratio 2, giving an effective resolution of $512 \times 512 \times 1536$, corresponding to a fine computational cell-width of approximately 59 microns, which was found to be adequate to resolve these lean hydrogen flames. Each simulation was initialized with a flat flame perturbed by a superposition of long wavelength Fourier modes. The flame was allowed to evolve without adaptive mesh refinement to allow the flame to become established at reduced expense. Refinement was then added to evolve a well-resolved set of statistically-stationary flames to provide the measurements discussed below.

Figure 2 shows the temperature field on a two-dimensional vertical slice of a 3cm$\times$3cm section of the freely-propagating flame simulation at an equivalence ratio of $\varphi = 0.40$. The thermodiffusive instability leads to the breakdown of the flat laminar flame, resulting in the cellular burning structure clearly visible in figure 2. The inset shows the local burning rate, where the peak is around 4 times the flat laminar flame value.

The freely-propagating flames were analyzed following the approach of [12]. Data were sampled from several time points in each simulation well after the steady flame was established and properly resolved. At each point, a flame surface was defined by first finding an isotherm close to the temperature corresponding to the peak heat release in the flat laminar flame (the diagnostic is insensitive to the precise value of temperature selected for this purpose). Integral curves of the temperature gradient are constructed in both directions from the isotherm, and form the boundaries of a local wedge-shaped volume cutting through the flame region. These curves extend in both directions well past where the local consumption rate falls below a threshold value. The union of the wedge-shaped volumes tiles the entire zone of hydrogen fuel consumption.

A local flame speed is evaluated by integrating the hydrogen consumption rate over each wedge-shaped volume, and normalizing the result by the mass density of hydrogen in the unburned fuel times the cross-sectional area of the volume at the flame isotherm. The local thermal thickness was evaluated along each integral curve by dividing the temperature jump across the flame by the peak temperature gradient along the curves. A single value for each wedge was defined as the average of the values from the three curves that bound it. The distribution of local flame speed and thermal thickness over the entire reaction zone is used to define the effective propagation speed, s_F, and effective thickness l_F. For this, we construct a PDF of each, weighted by the local consumption speed, and choose the peak value that results (i.e., we construct the speed and thickness where most of the flame is burning).

The weighted PDF plots of flame speed and thermal thickness are presented in figure 3. The solid vertical lines denote the peak values that were assigned as the characterizing parameters of the freely-propagating flame, s_F and l_F, and are listed in table 1. In all cases, the analysis confirms that the thermodiffusive instability leads to flames that burn more intensely and are locally thinner than the corresponding flat laminar flame. We see that $s_F/s_L \approx 2.1$ for $\varphi = 0.4$ and approximately 4.8 for $\varphi = 0.31$. Similarly, $l_F/l_L \approx 0.66$ for $\varphi = 0.4$ and approximately 0.29 for $\varphi = 0.31$. It is this variation with φ that is responsible for the lack of generality in Ka_L and Da_L for lean hydrogen. The modified Karlovitz and Damköhler numbers for the slices shown in figure 1 are given in table 1, where each case is lower than the corresponding laminar value, increasingly so with decreasing φ.

4 Turbulent Flame Simulations

In this section, we generate a family of statistically stationary turbulent flames using the s_F and l_F values developed in the previous section. The flame simulations were run following the approach taken in [7, 13]. Periodic lateral boundary conditions were specified, with a free-slip base and outflow at the top of the

domain. The background turbulent velocity field was maintained following [7, 13, 14] using a source term in the momentum equations. An inert calculation was run to establish the turbulence, and the reacting flow simulation was initialized by superimposing a laminar flame solution onto the turbulent velocity field. The base grid in each case was 64×64×256, with two levels of refinement used once the flame had become established, giving an effective resolution of 256×256×2048.

A new simulation was run for $\varphi = 0.40$ to match the conditions of case D31, where $\mathrm{Ka}_F = 79$. Specifically $L \approx 17.2 l_F$ and $\check{u} \approx 6.8 s_F$. These cases will be referred to as L31 and L40, where the L denotes the relatively low value of Ka_F. Figure 4 compares two-dimensional slices of density, burning rate and temperature for the cases at $\mathrm{Ka}_F = 79$ (note only five-eighths of domain height are shown). Note that peak temperatures are well above the adiabatic flame temperatures for the respective mixtures, indicating effects of the thermodiffusive processes. These flames are in the thin reaction zone. The two flames are clearly similar in structure; the turbulence tears off packets of fuel, but appears unable to disrupt the internal flame structure. The result is a sharp interface between fuel and products in both cases, and the burning occurs in small-scale structures over a broad flame brush.

Three additional simulations were run at $\varphi = 0.31$, 0.34 and 0.37 to match the conditions of D40, where $\mathrm{Ka}_F = 410$. Specifically, $L \approx 7.6 l_F$ and $\check{u} \approx 50 s_F$. These cases are labelled H31-H40 to denote the relatively high value of Ka_F. Figure 5 compares the slices of density, burning rate and temperature for the four cases. Density and temperature have been normalized by the laminar values, and the burning rate has been normalized by six times the peak laminar burning rate. Again, the turbulent flames appear similar to each other in structure (and distinctly different to the two simulations at $\mathrm{Ka}_F = 79$), and resemble a distributed flame (note that we will address specific diagnostics of the distributed regime in a forthcoming follow-on publication). Also, note that it is useful to normalize the slices in this case by the corresponding laminar flame parameters because the burning is in the distributed regime. Here, the values of temperature, for example, remain between the cold fuel and adiabatic flame temperatures, and in each case there appears to be no sharp interface between the fuel and the products. At the lowest equivalence ratio $\varphi = 0.31$, the flame appears to be significantly broader than the other three flames, although there is a slight decreasing trend in the turbulent flame width as equivalence ratio increases. Although the turbulent flames do not appear to be identical, the normalization by freely-propagating values appears to have made a vast improvement over normalization by flat laminar flame values.

5 Conclusions

For thermodiffusively-unstable low Lewis number flames, the freely propagating flame structure is significantly different than the idealized flat laminar flame, undermining the standard approach of characterizing turbulent flames in terms of Karlovitz and Damköhler numbers based on flat laminar flame properties. This was found to be a particular problem in the turbulent flame study of [7] (see figure 1 here), where turbulent flames at the same (laminar) Karlovitz and Damköhler number exhibited distinctly different behavior. In this paper, we have proposed an approach to rectify this shortcoming by measuring freely-propagating flame properties, thereby accounting for the flame response to its inherent instability in three dimensions. This was achieved through high-resolution three-dimensional simulations of lean premixed hydrogen flames at a variety of equivalence ratios, using the active control algorithm of [12]. Weighted probability density functions for flame speeds and thermal widths were used to assign effective flame properties based on freely propagating flame dynamics. Reevaluation of the Karlovitz numbers showed that in the leanest case Ka_L was almost 20 times Ka_F. Furthermore, Ka_F in the two extreme cases ($\varphi = 0.31$ and 0.40) differed by a factor of approximately 5.2. New simulations were run to match the freely-propagating Karlovitz and Damköhler numbers across the range of equivalence ratios. Conditions were chosen to match those of case D31 at $\mathrm{Ka}_F = 79$ using an equivalence ratio of $\varphi = 0.40$, and case D40 at $\mathrm{Ka}_F = 410$ using equivalence

ratios of $\varphi = 0.31$, 0.34, and 0.37. At $\mathrm{Ka}_F = 79$, a similar turbulent response was observed in both flames, the flame burns in narrow folded structures over a broad flame brush. At $\mathrm{Ka}_F = 410$, the flames were once again similar to each other, and markedly different than the $\mathrm{Ka}_F = 79$ flames; the latter flames appear to be burning in the distributed mode.

We acknowledge several shortcomings of the work presented here. A general warning in the turbulent premixed flame community is to avoid taking the regime diagrams too literally, in the sense that transitions between the various burning modes are not to be thought of as instantaneous. However, the variations we discuss here are hardly subtle. That being said, we should work to develop a more quantitative measure of the distributedness of a turbulent flame in order to concretely discuss this work in a broader context. This will be the focus of a forthcoming study, which extends this work to cover fuels over a larger range of Lewis numbers. Next, we acknowledge the omission of an important physical process in these flames due to the Soret effect. In fact, we suspect the Soret effect to have considerable influence on both s_F and l_F for ultra-lean hydrogen flames [15]. Particularly as we attempt to compare our work to experimental measurement, we expect that such terms will generate significantly larger scaling corrections. This paper represents a first attempt at quantifying the low-Le effects in the regime diagrams, and the effects discussed here can be explored in greater detail in future work.

Acknowledgments

MSD was supported by the DOE SciDAC Program. AJA and JBB were supported by the DOE Applied Mathematics Research Program. Simulations were performed on the Lawrencium cluster at LBNL, and Franklin at NERSC. All support is provided by the U.S. Department of Energy under Contract No. DE-AC02-05CH11231.

References

[1] G. H. Markstein, *The Journal of Chemical Physics* 17 (4) (1949) 428–429.

[2] Y. B. Zeldovich, *Theory of Combustion and Detonation in Gases (in Russian)*, Acad. Sci. USSR, 1944.

[3] B. Bregeon, A. S. Gordon, F. A. Williams, *Combustion and Flame* 33 (1978) 33–45.

[4] T. Mitani, F. A. Williams, *Combust. Flame* 39 (1980) 169–190.

[5] J. B. Bell, M. S. Day, R. K. Cheng, I. G. Shepherd, *Proc. Combust. Inst.* 31 (2007) 1309–1317.

[6] P. Strakey, T. Sidwell, J. Ontko, *Proc. Comb. Inst.* 31 (2007) 3173–3180.

[7] A. J. Aspden, M. S. Day, J. B. Bell, "Turbulence-Flame Interactions in Lean Premixed Hydrogen," (in preparation–available at `https://ccse.lbl.gov/people/aspden/index.html`).

[8] C. T. Bowman, *GRI-Mech 2.11*, available at `http://www.me.berkeley.edu/gri_mech`.

[9] M. S. Day, J. B. Bell, *Combust. Theory Modelling* 4 (2000) 535–556.

[10] J. B. Bell, M. S. Day, J. F. Grcar, *Proc. Combust. Inst.* 29 (2002) 1987–1993.

[11] J. B. Bell, M. S. Day, J. F. Grcar, M. J. Lijewski, *Comm. App. Math. Comput. Sci.* 1 (1) (2005) 29–52.

[12] M. S. Day, J. B. Bell, P.-T. Bremer, V. Pascucci, V. Beckner, M. J. Lijewski, *Combustion and Flame* 156 (5) (2009) 1035 – 1045.

[13] A. J. Aspden, J. B. Bell, M. S. Day, S. E. Woosley, M. Zingale, *The Astrophysical Journal* 689 (2008a) 1173–1185.

[14] A. J. Aspden, N. Nikiforakis, S. B. Dalziel, J. B. Bell, *Comm. App. Math. Comput. Sci.* 3 (1) (2008b) 101.

[15] J. F. Grcar, J. B. Bell, M. S. Day, *Proc. Combust. Inst.* 32 (2009) 1173–1180.

φ	0.31	0.34	0.37	0.40
s_L, cm/s	4.68	9.34	15.2	22.4
l_L, mm	1.9	1.1	0.79	0.63
s_F, cm/s	22.6	32.8	38.9	47.4
l_F, mm	0.55	0.47	0.44	0.41
Case	D31	D34	D37	D40
$\check{u}$, m/s	5.0	9.98	16.3	23.9
l, mm	0.95	0.55	0.395	0.314
L, mm	9.5	5.5	3.95	3.14
Ka_L	1560	1560	1560	1560
Da_L	4.7e-3	4.7e-3	4.7e-3	4.7e-3
Ka_F	79	155	284	410
Da_F	7.8e-2	3.9e-2	2.2e-2	1.5e-2
Case	H31	H34	H37	L40
$\check{u}$, m/s	11.4	16.5	19.6	10.5
l, m	0.42	0.36	0.33	0.71
L, m	4.2	3.6	3.3	7.1
Ka_L	8080	4105	2257	302
Da_L	9e-4	1.9e-3	3.2e-3	2.4e-2
Ka_F	410	410	410	79
Da_F	1.5e-2	1.5e-2	1.5e-2	7.8e-2
Δx, μm	16	14	13	28
η, μm	6.5	4.7	4.1	19
η_e, μm	8.1	6.4	5.7	20

Table 1: Simulation properties.

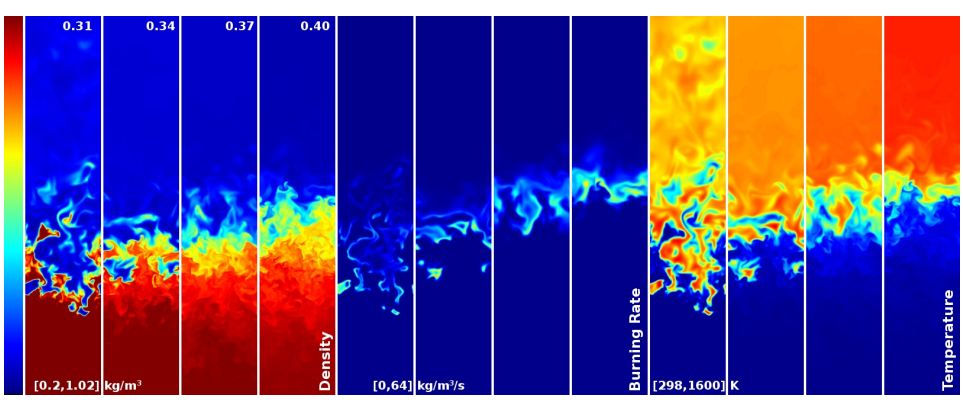

Figure 1: Two-dimensional slices of three-dimensional simulations of lean-premixed hydrogen for cases D31-D40.

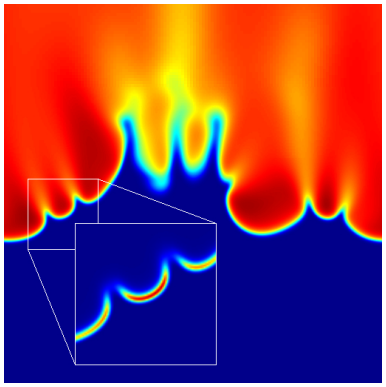

Figure 2: Temperature slice of a 3cm$\times$3cm section of the freely-propagating flame simulation at $\varphi = 0.40$. The inset shows the burning rate, where the peak burning rate is approximately 4 times that of the flat laminar flame.

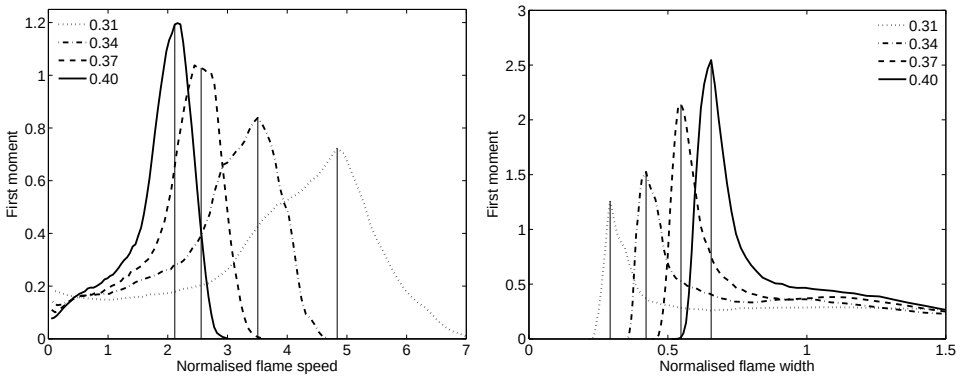

Figure 3: First moments of the probability density functions for normalized local flame speed (top) and width (bottom) for the freely-propagating flames.

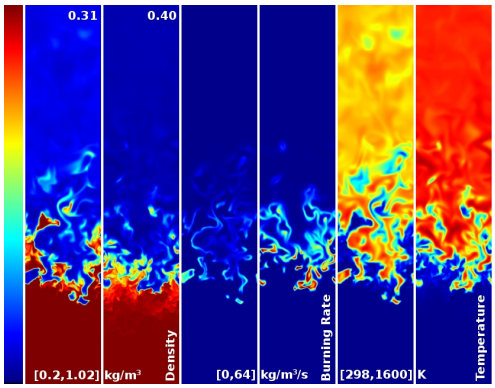

Figure 4: Two-dimensional slices of density, burning rate and temperature for cases L31 and L40.

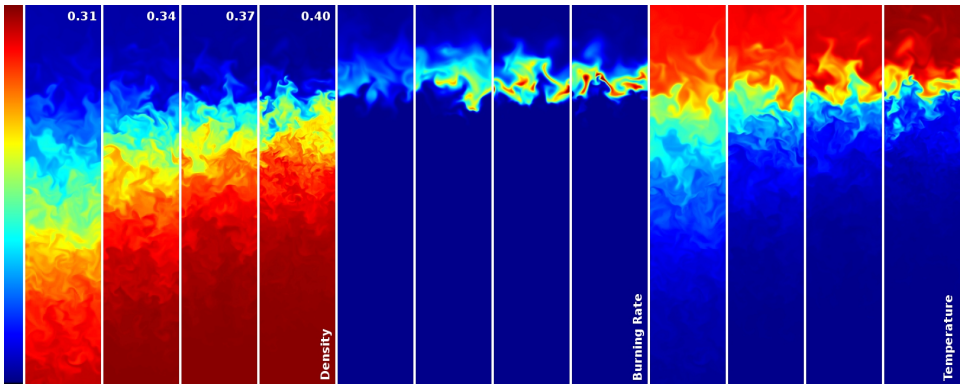

Figure 5: Two-dimensional slices of density, burning rate and temperature for cases H31-H37. The density and temperature have been normalized by the corresponding laminar values, and the burning rate has been normalized by six times the peak laminar burning rate.